

# Energy release rate analysis for adhesive and laminate double cantilever beam specimens emphasizing the effect of residual stresses

John A. Nairn\*

*Department of Material Science and Engineering, University of Utah, 122 S. Central Campus Drive, Room 304  
Salt Lake City, UT 84112-0560, USA*

Received 6 November 1996

---

## Abstract

The mode I energy release rate, including the effect of residual stresses, was evaluated for both adhesive and laminate double cantilever beam specimens. The energy release rate can be partitioned into a mechanical term and a residual stress term in beam theory. The beam-theory mechanical term is not very accurate, but can be corrected by a slight modification to a previous correction factor. This correction factor accounts for crack tip rotation of the specimen arms. The beam-theory residual stress term is very accurate for a wide range of specimen geometries; it can be used without correction. The consequence of ignoring residual stresses is that one measures an *apparent* toughness instead of a *true* toughness. The error between the apparent toughness and true toughness can be calculated for a given specimen geometry and amount of residual stresses. Such errors can be large and are often larger than the correction required for crack-tip rotation effects. In double cantilever beam specimens used to study laminate delamination, the errors are large when the delaminating arms, considered by themselves, are unsymmetric laminates. Some experimental methods are suggested which can be used to correct for residual stress effects.

*Keywords:* Adhesive Toughness, Fracture Mechanics, Residual Stresses, Delamination

---

## 1. Introduction

Since the work of Mostovoy, Ripling, *et al.* [1–3], the double cantilever beam (DCB) specimen geometry has been a popular method for measuring the fracture toughness of adhesive bonds and delamination fracture toughness of composite laminates. There are existing standard protocols for mode I testing of both adhesive bonds [4] and laminate delamination [5]. The same specimen geometry with modified loading methods can be used for the study of mode II and mixed mode fracture as well [6, 7]. There are ongoing efforts to refine adhesive fracture and delamination methods to give the best possible results [8]. These standards, however, do not address methods for dealing with residual stresses. When adhesive joints are cured, or laminates are processed, at high temperature and then cooled to room temperature, residual stresses will inevitably be present. These stresses can arise either from differential thermal shrinkage between the components of the specimen or from chemical shrinkage of the adhesive or composite matrix resins. When a crack grows in a specimen with residual stresses, the residual stresses can contribute to the total amount of energy released. If residual stress effects are ignored, the calculated fracture toughness will not be the *true* fracture toughness. Instead, it will be an *apparent* toughness that includes a specimen property (the amount of residual stresses) within the desired material property (the toughness). When such an apparent toughness is used for prediction of failure in adhesive joints that have different levels of residual stresses, those predictions will not be correct. Furthermore, the most common residual stress effect in adhesive DCB specimens is for

---

\*Tel: +1-801-581-3413; fax: +1-801-581-4816.

*E-mail address:* John.Nairn@m.cc.utah.edu (J.A. Nairn)

the *apparent* toughness to be larger than the *true* toughness. Thus, adhesive designs based on such non-conservative *apparent* toughnesses could lead to premature failure.

This paper describes a mode I energy release rate analysis for crack growth in adhesive DCB specimens and laminate delamination specimens. The thermoelastic energy release rate analysis uses linear-elastic beam theory. Large-displacement, end-block loading, and plasticity effects were ignored, but these effects could be included by methods developed previously for delamination [7, 9] and adhesive fracture [10] analysis. The crack is assumed to propagate straight; for adhesives, it is therefore assumed to remain in the middle of the adhesive as a cohesive mode I fracture. The energy release rate can be partitioned into two terms — a term involving mechanical loads and a term involving residual stresses. The accuracy of each term was studied by extensive finite element calculations. As observed in previous work, the beam-theory mechanical term is inaccurate because it ignores arm rotation at the root of the crack [7, 10, 11]. A previously-published correction to the mechanical term [10] is very accurate, provided it is multiplied by a numerically-determined constant. In contrast, the beam-theory residual stress term is accurate, without correction, for a wide range of specimen geometries.

From the accurate residual stress term, it is possible to calculate the error induced in the measured fracture toughness for any DCB specimen, if residual stresses are ignored. The error in adhesive DCB specimens can be significant. It gets smaller as the adhesive layer gets thinner and as the modulus ratio between the adherend and the adhesive gets larger. In laminate DCB specimens, the residual effect disappears if both arms of the DCB specimen are themselves symmetric laminates. If the arms are not symmetric laminates, the residual stress effect will generally be significant.

Finally, accounting for residual stresses in analysis of DCB specimens requires knowledge of the level of residual stresses in the specimen. Some experimental methods based on calibration specimens, on observing initial beam curvatures, or on the load-displacement curve are discussed. The recommended method is to extrapolate the residual stress term from a properly-zeroed, load-displacement curve. Although the energy release rate analysis is specific for residual thermal stresses, the experimental correction method is general; it can account for any type of residual stresses.

## 2. General energy release rate analysis

Figure 1 shows a double cantilever beam (DCB) specimen geometry used to measure the mode I toughness of adhesive bonds. In a fracture mechanics analysis of this specimen, the crack is predicted to propagate when the thermoelastic energy release rate for mode I crack growth ( $G_I$ ) becomes equal to the toughness of the adhesive or the adhesive's critical energy release rate ( $G_{Ic}$ ). The mechanics problem is thus to find  $G_I$  including the effect of residual stresses. A recent paper [12] has derived an exact result for mode I energy release rate in any composite with residual stresses:

$$G_I = \left( \sqrt{G_{mech}} + \frac{1}{2} \frac{\frac{d}{dA} \int_V \boldsymbol{\sigma}^m \cdot \boldsymbol{\alpha} \Delta T dV}{\sqrt{G_{mech}}} \right)^2 \quad (1)$$

where  $G_{mech}$  is the energy release rate in the absence of residual stresses,  $\boldsymbol{\sigma}^m$  is the stress tensor due to mechanical loads only,  $\boldsymbol{\alpha}$  is the position-dependent thermal expansion tensor of the composite material, and  $\Delta T = T_s - T_0$  is the temperature difference between specimen test temperature ( $T_s$ ) and the stress-free temperature ( $T_0$ ). The derivative in the numerator is with respect to total crack area  $A$ . In this analysis, the adhesive DCB specimen is treated as a two-phase composite with the two phases being the adhesive joint and the two adherends. Equation (1) was derived using a linear thermoelasticity analysis. It assumes residual stresses arise due to differential thermal shrinkage between the phases of the specimen under a uniform change in temperature of  $\Delta T$  [12]. Some experimental methods to correct for other types of residual stresses are discussed below.

For the traction-only loading of the adhesive DCB specimen (see *Figure 1*), some further results from Ref. 12 are that

$$G_{mech} = \frac{1}{2} \frac{d}{dA} \int_S \vec{T}^0 \cdot \vec{u}^m dS \quad \text{and} \quad \int_V \boldsymbol{\sigma}^m \cdot \boldsymbol{\alpha} \Delta T = \int_S \vec{T}^0 \cdot \vec{u}^r dS \quad (2)$$

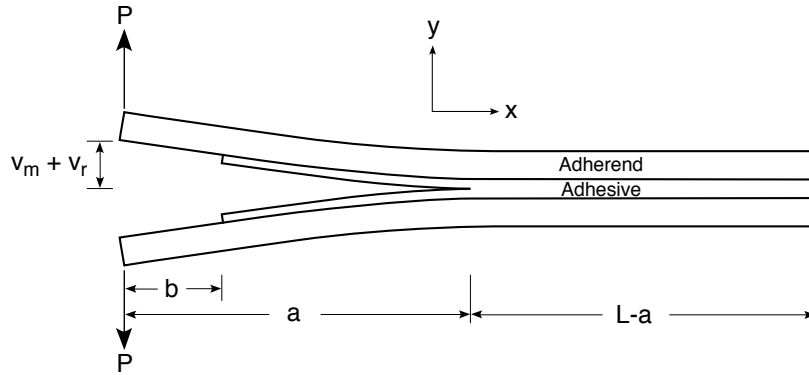


Fig. 1. A double cantilever beam specimen used to measure the mode I toughness of adhesive bonds. The cantilever arm length is  $a$ , the total specimen length in  $L$ . Sometimes the adhesive does not extend to the end of the arms; here the adhesive stops a distance  $b$  from the ends.

where  $\vec{T}^0$  is the applied surface traction,  $\vec{u}^m$  and  $\vec{u}^r$  are the displacements due to mechanical or residual stresses, respectively. For a  $2D$ , plane-stress analysis (all stresses in the  $z$  direction assumed to be zero), the tractions applied to the DCB specimen are

$$\vec{T}^0 = \frac{P}{B} \delta(\vec{x} - \vec{x}_u) - \frac{P}{B} \delta(\vec{x} - \vec{x}_l) \tag{3}$$

where  $P$  is the total applied load,  $B$  is the specimen thickness in the  $z$  direction,  $\delta(\vec{x})$  is the Dirac delta function, and  $\vec{x}_u$  and  $\vec{x}_l$  are the locations of the upper and lower loading points. Substitution of this traction vector into equations (1) and (2) with  $dA = B da$ , where  $a$  is the DCB specimen arm length, leads to

$$G_I = \left( \sqrt{G_{mech}} + \frac{P \frac{dv_r}{da}}{\sqrt{G_{mech}}} \right)^2 \quad \text{and} \quad G_{mech} = \frac{P}{B} \frac{dv_m}{da} \tag{4}$$

where  $v_m$  and  $v_r$  are the load point displacements at the top loading point ( $\vec{x}_u$ ) in the  $y$  direction due to mechanical or residual stresses, respectively (see *Figure 1*).

In general, residual stresses can contribute to energy release rate either by releasing strain energy or by doing external work as the crack grows [12]. The residual stress contribution to energy release rate here is the second term in equation (4). It is immediately seen to be equal to the external work caused by changes in residual displacements ( $v_r$ ) under load  $P$  at the loading points. In other words, the entire effect of residual stresses in DCB specimens is an external work effect arising from thermally induced curvature in the DCB arms. Although the full DCB specimen is a balanced structure, each DCB arm is an unbalanced, two-layer structure. As the crack grows, the unbalanced arms may curve due to residual stresses; this curvature leads to external work that causes the entire residual stress effect in  $G_I$ .

By equation (4), the analysis for  $G_I$  is reduced to finding the loading point mechanical and residual displacements. Here one arm of the specimen will be analyzed by simple beam theory. We begin by writing the upper-arm, moment-curvature-temperature relation as

$$\kappa = \frac{d^2v}{dx^2} = C_\kappa^* M + \alpha_\kappa^* \Delta T \tag{5}$$

where  $\kappa$  is beam curvature (defined as positive for curvature upwards),  $v$  is  $y$ -direction displacement,  $M$  is the applied moment,  $C_\kappa^*$  is the *effective* beam bending compliance, and  $\alpha_\kappa^*$  is the *effective* beam thermal-curvature coefficient. In common adhesive specimens, the adhesive joint does not extend all the way to the loading point as shown in *Figure 1* where the adhesive stops at a distance  $b$  from the end. An analysis for finding beam displacements must account for the different values of  $C_\kappa^*$  and  $\alpha_\kappa^*$  in the region with adhesive and the region with no adhesive. Because  $b$  remains constant, however, as the crack propagates, the beam

section with no adhesive makes a constant contribution to displacements that drops out when derivatives with respect to  $a$  are evaluated. In other words,  $G_I$  is independent of  $b$ ; for simplicity we can evaluate load-point displacements by setting  $b = 0$ . Integration of equation (5) for mechanical stresses only ( $M = Px$ ,  $\Delta T = 0$ , and  $x = 0$  at the loading point) or residual stresses only ( $M = 0$ ,  $\Delta T \neq 0$ ) leads to

$$v_m = \frac{1}{3}C_{\kappa}^*Pa^3 \quad \text{and} \quad v_r = \frac{1}{2}\alpha_{\kappa}^*\Delta Ta^2 \quad (6)$$

Substituting loading-point mechanical and residual displacements into equation (4) gives

$$G_I = (C_m Pa + C_r \Delta T)^2 \quad (7)$$

where

$$C_m = \sqrt{\frac{C_{\kappa}^*}{B}} \quad \text{and} \quad C_r = \frac{\alpha_{\kappa}^*}{\sqrt{C_{\kappa}^* B}} \quad (8)$$

The  $G_I$  analysis has been reduced to the problem of finding the effective beam properties of the cantilever arms. Specific results for adhesive or laminate DCB specimens are given in the following two sections.

In many adhesive DCB specimens, such as those with polymeric adhesives and metallic adherends,  $\alpha_{\kappa}^*\Delta T$ , and hence  $v_r$ , will be negative. This fact seems to invalidate the residual displacement analysis because it corresponds to the upper arm displacing down and through the lower arm. The  $G_I$  analysis, however, remains valid provided the *total* beam displacement,  $v = v_m + v_r$ , is positive; in other words, the analysis remains valid for any adhesive DCB test where the beam arms must be mechanically opened to induce fracture. The situation where the crack grows without  $v$  being positive corresponds to a specimen that fails due to residual stresses alone and therefore to a specimen that would not be used in a subsequent adhesive fracture test.

### 3. Adhesive double cantilever beam specimens

Analysis of adhesive DCB specimens was reduced above to finding the effective beam properties,  $C_{\kappa}^*$  and  $\alpha_{\kappa}^*$ , both of which can be found by simple composite beam analyses. The preferred, but still simple, analysis is one that considers the full beam geometry or one that does not assume the adhesive is thin. The coordinates for analysis of one adhesive DCB arm are shown in *Figure 2*. By simple beam analysis (*e.g.*, Ref. 13)

$$C_{\kappa}^* = \frac{1}{(EI)_{effective}} = \frac{1}{E_1 I_{zz,1} + E_2 I_{zz,2}} \quad (9)$$

where  $E_i$  and  $I_{zz,i}$  are the modulus and moment of inertia about the neutral axis for phase  $i$  ( $i = 1$  for the adherend and  $i = 2$  for the adhesive). The neutral axis is located at

$$y_N = \frac{h_1 h_2}{2} \frac{E_1 - E_2}{E_1 h_1 + E_2 h_2} \quad (10)$$

where  $h_1$  and  $h_2$  are the thicknesses of the adherend and adhesive, respectively. By the parallel axis theorem

$$I_{zz,1} = \frac{Bh_1^3}{12} + Bh_1 \left( y_N - \frac{h_2}{2} \right)^2 \quad \text{and} \quad I_{zz,2} = \frac{Bh_2^3}{12} + Bh_2 \left( y_N + \frac{h_1}{2} \right)^2 \quad (11)$$

The beam  $C_{\kappa}^*$  can be written in a convenient form as

$$C_{\kappa}^* = \frac{12}{E_1 B h_1^3} \frac{\lambda^2 (1 + R\lambda)}{3(1 + \lambda)^2 + (1 + R\lambda) \left( \lambda^2 + \frac{1}{R\lambda} \right)} \quad (12)$$

where

$$R = \frac{E_1}{E_2} \quad \text{and} \quad \lambda = \frac{h_1}{h_2} \quad (13)$$



Fig. 2. The coordinate system used for composite beam analysis of one arm of an adhesive DCB specimen.

The result for  $\alpha_{\kappa}^*$  is the classic Timoshenko, bimetallic strip problem [14] which can be written as

$$\alpha_{\kappa}^* = -\frac{6\Delta\alpha(1 + \lambda)}{h_2 \left( 3(1 + \lambda)^2 + (1 + R\lambda) \left( \lambda^2 + \frac{1}{R\lambda} \right) \right)} \tag{14}$$

where  $\Delta\alpha = \alpha_1 - \alpha_2$  is the difference in thermal expansion coefficients between the adherend and the adhesive. For typical polymeric adhesives with metallic adherends,  $\alpha_1 < \alpha_2$  and  $\Delta T < 0$  as the specimen cools from the cure temperatures to the testing temperature. For such specimens,  $\alpha_{\kappa}^* \Delta T < 0$ , and the residual stresses cause the beam arms to bend towards the center of the specimen. Thus, in such specimens, the residual stresses cause the beam arms to do work on the loading system.

From equation (8), the mechanical and residual coefficients for determining  $G_I$  are

$$C_m = \frac{2\lambda}{Bh_1} \sqrt{\frac{3(1 + R\lambda)}{E_1 h_1 \left( 3(1 + \lambda)^2 + (1 + R\lambda) \left( \lambda^2 + \frac{1}{R\lambda} \right) \right)}} \tag{15}$$

$$C_r = -\Delta\alpha(1 + \lambda) \sqrt{\frac{3E_1 h_1}{(1 + R\lambda) \left( 3(1 + \lambda)^2 + (1 + R\lambda) \left( \lambda^2 + \frac{1}{R\lambda} \right) \right)}} \tag{16}$$

### 3.1. Comparison to finite element results

For judgement of the accuracy of  $C_m$  and  $C_r$ , a large number of finite element calculations (FEA) were done in which  $R$  was varied from 1 to 100 and  $\lambda$  was varied from 1 to 128. The accuracy of beam theory depends on the axial ratio of the beam arms; thus for each pair of  $R$  and  $\lambda$ , analyses were done for arm axial ratios ( $a/h$ ) from 2.5 to 160. For these calculations, the adhesive properties were held constant at  $E_2 = 2500$  MPa,  $\nu_2 = 0.35$ , and  $\alpha_2 = 60 \times 10^{-6} \text{ K}^{-1}$ ; the adherend modulus was  $E_1 = RE_2$  while  $\nu_1 = 0.3$  and  $\alpha_1 = 20 \times 10^{-6} \text{ K}^{-1}$  were held constant. The arm geometry (see *Figures 1 and 2*) was set to  $h = 5$  mm and  $L = 2a = 2h(a/h)$ ; the analysis is independent of  $B$ . The composite beam was meshed into 8-noded, isoparametric, quadrilateral elements with mid-side nodes. The energy release rate,  $G_I$ , was calculated by crack closure methods [15]. With square crack-tip elements, it was possible to get accurate results even with relatively coarse meshes. All results reported here were for a sufficiently refined mesh of about 600 elements and 2000 nodes.

As expected, the errors in beam-theory  $C_m$  and  $C_r$  got larger as the arm axial ratio got smaller. At constant  $a/h$ , however, the relative errors in  $C_m$  and  $C_r$  were approximately independent of  $R$  and  $\lambda$ . The absolute value of the errors in  $C_m$  or  $C_r$ , averaged for  $\lambda$  from 1 to 128, are plotted as a function of  $a/h$  in *Figure 3*. *Figure 3* is for  $R = 28$  which corresponds to aluminum adherends ( $E_1 = 70000$  MPa) with a typical epoxy adhesive ( $E_2 = 2500$  MPa). The results for any other value of  $R$  (from 1 to 100) were similar, except that the errors for small  $a/h$  grew slightly at larger values of  $R$ .

The errors in the residual stress coefficient,  $C_r$ , were always less than 1% for  $a/h > 5$  and were typically less than 0.01% for  $a/h > 10$ . For  $a/h < 5$ , the errors were still low for  $R < 20$ , but got larger and depended on  $\lambda$  for  $R > 20$ . Thus, except for the combination of  $a/h < 5$  and  $R > 20$ , the simple beam theory result for  $C_r$  does an excellent job of evaluating the contribution of residual stresses to total energy release rate.

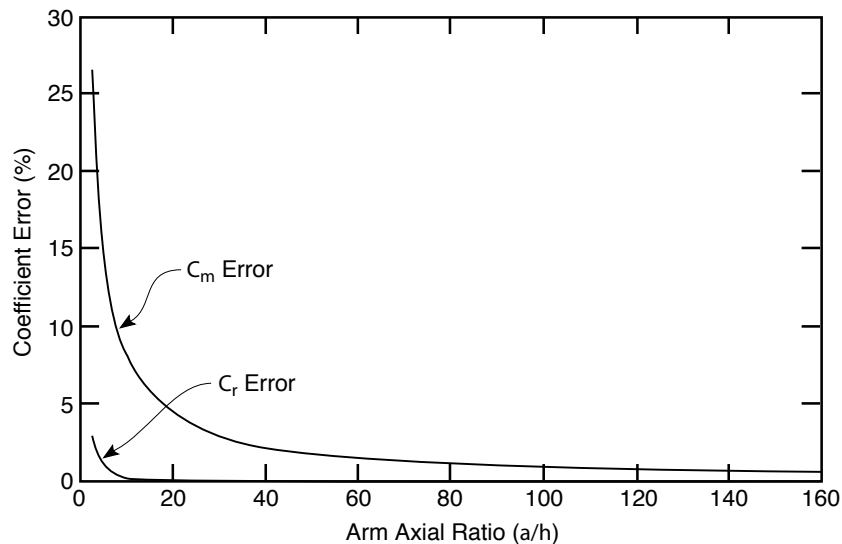


Fig. 3. The average or the absolute values of the errors between the theoretical coefficients  $C_m$  and  $C_r$  and the mechanical and residual stress results calculated by FEA as a function of the arm axial ratio. These results are for  $R = 28$ . For each arm axial ratio, the error was averaged for  $\lambda$  from 1 to 128.

Because typical adhesive DCB specimens strive to use long, slender arms (large  $a/h$ ), the residual stress correction evaluated here should be sufficiently accurate for all commonly-used adhesive fracture specimens.

The errors in  $C_m$  normally exceeded 1% and got very large for small  $a/h$ . This observed error in simple beam theory for calculating mechanical energy release rate has been discussed before [7–10]. The error is caused by an over-simplification in the simple beam theory analysis that prevents rotation of the specimen arms at the crack tip; for accurate analysis, this rotation can not be ignored. Williams analyzed an adhesive DCB specimen ignoring residual stresses [10]. He wrote a corrected mechanical beam theory result as

$$G_I(\Delta T = 0) = (C_m^\infty (a + \Delta_W) P)^2 \quad \text{where} \quad C_m^\infty = \lim_{\lambda \rightarrow \infty} C_m = \sqrt{\frac{12}{EB^2 h_1^3}} \quad (17)$$

is the limiting mechanical energy release rate coefficient for a very thin adhesive. In other words, the corrected analysis replaces the true crack length,  $a$ , by an effective crack length,  $a + \Delta_W$ . Using the beam-on-elastic-foundation model of Kanninen [16], Williams derived the effective crack length correction in terms of specimen properties to be

$$\Delta_W = h_1 \left( \frac{1 + \frac{R}{\lambda}}{6} \right)^{1/4} \quad (18)$$

If  $G_I^{FEA}$  is the energy release rate calculated by finite element analysis with  $\Delta T = 0$ , a numerically-determined effective crack length correction for equation (17) can be found from

$$\Delta_{FEA}^\infty = \frac{\sqrt{G_I^{FEA}}}{C_m^\infty P} - a \quad (19)$$

When including specimens with possibly thick adhesive layers, however, it is preferable to find the effective crack length correction relative to the full composite beam analysis for  $C_m$  rather than for the thin-adhesive beam result of  $C_m^\infty$ . In other words, here the FEA effective crack length correction was found from

$$\Delta_{FEA} = \frac{\sqrt{G_I^{FEA}}}{C_m P} - a \quad (20)$$

When this numerically-calculated  $\Delta_{FEA}$  was compared to the theoretical  $\Delta_W$  in equation (18) for all finite element calculations, they were found to be related by an almost constant ratio of

$$\frac{\Delta_{FEA}}{\Delta_W} = 1.15 \quad (21)$$

This ratio was independent of  $\lambda$  (in the range of 1 to 128) and  $a/h$  (in the range 2.5 to 160). The ratio was weakly dependent on  $R$  — it was independent of  $R$  for  $R > 5$  and increased slightly at low  $R$ , reaching 1.20 when  $R = 1$ . No attempt was made to derive the origin of the constant ratio of  $\Delta_{FEA}$  to  $\Delta_W$ . The beam-on-elastic foundation analysis in Ref. 10 ignored shear stresses although it was noted they could be added using the methods of Ref. 11. Because shear corrections depend on beam axial ratio while the results here were independent of arm axial ratio, it is unlikely that shear effects account for the discrepancy. Simple beam theory is one dimensional and thus does not account for Poisson ratio mismatch effects. To test for an effect of  $\nu_1 - \nu_2$  on the correction ratio, some additional calculations were done for  $R = 28$  and  $\nu_1$  varying from -0.95 to +0.45. Again, there was no effect on the  $\Delta_{FEA}/\Delta_W$  ratio. The numerical result of  $1.15\Delta_W$  can thus be regarded as a numerically-determined correction factor valid for any typical adhesive DCB specimen with isotropic layers.

Using the numerically-determined adjustment to  $\Delta_W$ , the energy release rate can be written as

$$G_I = \left( C_m \left( 1 + 1.15 \frac{\Delta_W}{a} \right) P a + C_r \Delta T \right)^2 \quad (22)$$

The average errors for all values of  $a/h \geq 2.5$  were less than 1% and typically much less than 1%. The maximum errors in the mechanical term occurred for small  $R$  while the maximum errors in the residual stress term occurred for large  $R$ . Even these *maximum* errors, however, were smaller than 1%, provided  $a/h \geq 10$ .

### 3.2. Consequence of ignoring residual stresses

Many previous adhesive toughness experiments have ignored residual stresses. The energy release rate result in equation (22) can be used to calculate the errors of such an approach. Assume that some particular adhesive has a *true* fracture toughness of  $G_{Ic}$ . If an adhesive DCB specimen with this adhesive is tested, it will fail when  $G_I = G_{Ic}$ , which occurs when

$$P = \frac{\sqrt{G_{Ic}} - C_r \Delta T}{C_m(a + 1.15\Delta_W)} \quad (23)$$

Notice that  $P < 0$  if  $G_{Ic} < C_r^2 \Delta T^2$ . This condition corresponds to a DCB specimen that fails due to residual stresses alone. If the observed failure load is then used in an analysis that ignores residual stresses (equation (22) with  $\Delta T = 0$ ), the *apparent* toughness and its percent error relative to the *true*  $G_{Ic}$  would be

$$G_{Ic}^{app} = \left( \sqrt{G_{Ic}} - C_r \Delta T \right)^2 \quad \text{and} \quad G_{Ic}^{app} \text{ Error} = 100 \left[ \left( 1 - \frac{C_r \Delta T}{\sqrt{G_{Ic}}} \right)^2 - 1 \right] \quad (24)$$

This error, or consequence of ignoring residual stresses, can be calculated without knowledge of  $C_m$  or  $\Delta_W$ .

For a sample calculation of errors due to ignoring residual stresses, we considered an adhesive with  $G_{Ic} = 200 \text{ J/m}^2$  and residual stresses due to  $\Delta\alpha = -40 \times 10^{-6} \text{ K}^{-1}$  and  $\Delta T = -100^\circ\text{C}$ . These parameters correspond to a typical high-temperature cure epoxy adhesive bonded to metallic adherends. The total differential strain of  $\Delta\alpha\Delta T = 0.40\%$  is not excessively large for adhesive specimens. Because  $C_r\Delta T < 0$ ,  $G_{Ic}^{app}$  will be *higher* than the true toughness. *Figure 4* plots the percentage error in  $G_{Ic}^{app}$  as a function of  $R$  for various  $\lambda$  from 2 to 64. The errors are extremely large for low  $R$  and low  $\lambda$  and decrease as either  $R$  or  $\lambda$  increase. In general, the errors are never insignificant. The dashed vertical line shows a typical  $R$  value for aluminum-epoxy specimens ( $R = 28$ ). Despite the high aluminum-epoxy  $R$  value, the errors exceed 1% even with a very thin adhesive ( $\lambda = 64$ ). The errors in aluminum-epoxy specimens increase to over 40% as  $\lambda$  decreases to 2. Finally, the errors depend on total arm thickness ( $h$ ). The results in *Figure 4* were for  $h = 5 \text{ mm}$ ; the errors increase for specimens with larger  $h$ .

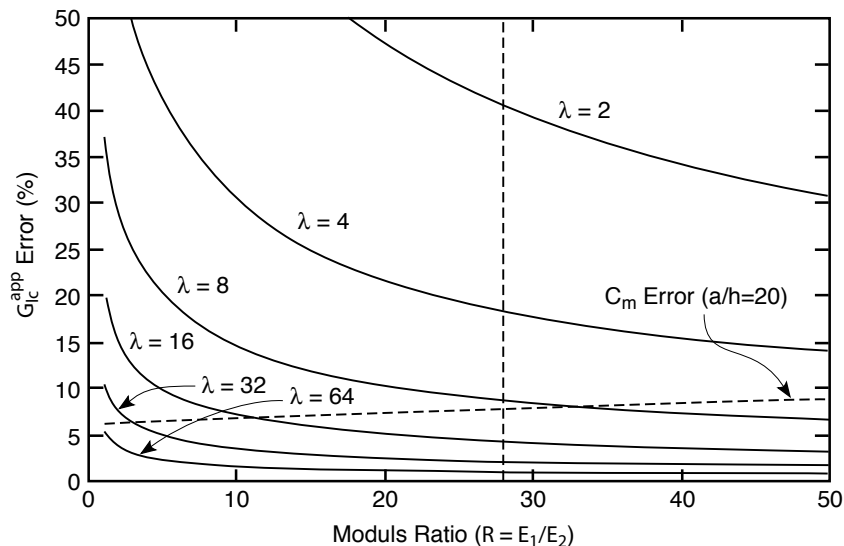


Fig. 4. The error in  $G_{Ic}^{app}$  when residual stresses are ignored as a function of  $R$  for various values of  $\lambda$ . The adhesive DCB specimens were assumed to have  $h = 5$  mm,  $G_{Ic} = 200$  J/m<sup>2</sup>,  $\Delta\alpha = -40 \times 10^{-6}$  K<sup>-1</sup>, and  $\Delta T = -100^\circ$ C. The vertical dashed line corresponds to  $R = 28$  which is a typical value for aluminum-epoxy specimens. The nearly-horizontal dashed line gives the errors caused in the mechanical energy release rate when ignoring the crack-length correction term for beam arms with  $a/h = 20$ .

Early work on adhesive fracture using DCB specimens investigated the effects of adhesive joint thickness, DCB specimen width, and post-cure temperature [1–3] on toughness, but these experiments ignored residual stresses and thus actually observed changes in  $G_{Ic}^{app}$  instead of the *true*  $G_{Ic}$ . Interestingly, all experimentally observed trends in  $G_{Ic}^{app}$  match predicted trends if we assume all changes are due solely to a change in level of residual stresses. As the adhesive joint gets thicker,  $\lambda$  get smaller which increases the residual stress effect and causes  $G_{Ic}^{app}$  to increase; this prediction matches experiments [2, 3]. As the DCB specimen width changes, there should be no effect on  $G_{Ic}^{app}$ ; this prediction matches experiments [3]. As the post-cure temperature increases,  $\Delta T$  gets more negative, which increases the residual stresses and causes  $G_{Ic}^{app}$  to increase; this prediction matches experiments [2, 3]. The magnitude of the observed  $G_{Ic}^{app}$  changes with joint thickness and post-cure temperature [2, 3] are probably larger than can be accounted for by a residual stress effect alone. It is likely, however, that residual stresses account for a non-negligible fraction of the changes. The most appropriate physical picture of the changes in toughness should be derived from the true  $G_{Ic}$  instead of from  $G_{Ic}^{app}$ . In one paper on post-cure temperature effects, Mostovoy and Ripling [2] concluded that residual stresses are not important because  $G_{Ic}^{app}$  increased with post-cure temperature while they expected that an increased level of residual stress could only cause  $G_{Ic}^{app}$  to decrease. This assessment is incorrect; in typical polymeric adhesives with metallic adherends, increasing the level of residual stresses causes  $G_{Ic}^{app}$  to increase.

Much effort has gone into corrections to the beam-theory mechanical term in proposing standards for mode I fracture of adhesive specimens [8, 10]. It is therefore interesting to compare the magnitude of the errors induced by ignoring the mechanical correction to those induced by ignoring residual stresses. If we consider a specimen with no residual stresses and a true toughness of  $G_{Ic}$ , by a similar procedure applied to analysis of residual stress errors, the percent error in the apparent toughness with respect to the true toughness caused by ignoring the mechanical term correction factor is

$$G_{Ic}^{app} \text{ Mechanical Error} = 100 \left[ \left( \frac{a}{a + 1.15\Delta W} \right)^2 - 1 \right] \quad (25)$$

This error is nearly independent of  $\lambda$ , but is a strong function of  $a/h$  and a weak function of  $R$ . Superimposed on *Figure 4* is the mechanical error of typical adhesive specimens with  $a/h = 20$ . For an aluminum/epoxy specimen ( $R = 28$ ), the residual stress error is larger than the mechanical error for thicker adhesives ( $\lambda < 10$ ), but gets smaller for thinner adhesives ( $\lambda > 10$ ). As  $a/h$  gets larger, the mechanical errors get smaller while

the residual stress errors do not change. Thus, for larger  $a/h$ , the residual stress errors will usually be larger than the mechanical errors. The exact value of the residual stress error depends on specimen geometry and the level of residual stresses in the adhesive, but in ordinary adhesive specimens it will often have a magnitude similar to the error induced by ignoring crack tip rotation. It makes little sense to carefully correct for all mechanical effects while ignoring a similar-magnitude residual-stress error, especially since the residual stress effect can be accurately included by use of the  $C_r \Delta T$  term in the energy release rate expression in equation (22).

### 3.3. Asymptotic results for thin adhesives

Many analyses of adhesive specimens assume the adhesive is thin. To judge the conditions for which the thin-adhesive limit is valid, we derived asymptotic expansions for  $C_m$ ,  $C_r$ , and  $\Delta_W$  and compared those results to the full composite beam results. Expanding all results in a Taylor series in  $1/\lambda$  and truncating after the linear terms gives the following asymptotic results:

$$C_m (\lambda \text{ large}) = \sqrt{\frac{12}{E_1 B^2 h_1^3}} \left(1 - \frac{3}{2R\lambda}\right) + O[1/\lambda^2] \quad (26)$$

$$C_r (\lambda \text{ large}) = -\frac{\Delta\alpha}{R\lambda} \sqrt{3E_1 h_1} + O[1/\lambda^2] \quad (27)$$

$$\Delta_W (\lambda \text{ large}) = 0.638943h_1 \left(1 + \frac{R}{4\lambda}\right) + O[1/\lambda^2] \quad (28)$$

The constant term in each limiting expression is the result as  $\lambda \rightarrow \infty$ :

$$C_m^\infty = \lim_{\lambda \rightarrow \infty} C_m = \sqrt{\frac{12}{E_1 B^2 h_1^3}}, \quad C_r^\infty = \lim_{\lambda \rightarrow \infty} C_r = 0, \quad \text{and} \quad \Delta_W^\infty = \lim_{\lambda \rightarrow \infty} \Delta_W = 0.638943h_1 \quad (29)$$

Notice that in the limit of no adhesive, there will be no beam curvature due to mismatched thermal expansion coefficients and thus the residual stress effect vanishes ( $C_r^\infty = 0$ ).

Figure 5 plots  $C_m (\lambda \text{ large})$ ,  $C_m^\infty$ ,  $C_r (\lambda \text{ large})$ ,  $\Delta_W (\lambda \text{ large})$ , and  $\Delta_W^\infty$  as a function of  $\lambda$  for a typical aluminum-epoxy specimen. Each limiting result has been normalized to the full composite beam results in equations (15), (16), and (18) and thus deviations from 1 give the error caused by use of a limiting result rather than the full result. The limiting result  $C_r^\infty$  is not plotted because it is always zero. Both  $C_m (\lambda \text{ large})$  and  $C_m^\infty$  converge very rapidly and agree within 1% with the full beam analysis, provided  $\lambda > 10$ . All other constants converge more slowly.  $C_r (\lambda \text{ large})$  and  $\Delta_W (\lambda \text{ large})$  require  $\lambda > 80$  to be within 1% of the full beam analysis while  $\Delta_W^\infty$  requires  $\lambda > 700$ . Figure 5 is for  $R = 28$ . The  $C_m$  results converge faster as  $R$  gets larger while the  $\Delta_W$  results converge slower. The  $C_r$  convergence is relatively insensitive to  $R$ . In summary, it is acceptable to use thin-adhesive, asymptotic results for  $C_m$ , provided  $\lambda$  is larger than about 10 and  $R$  is not too small. For typical adhesive DCB specimens, however, it is not accurate to use the thin-adhesive limits for either  $C_r$  or  $\Delta_W$ . The full expressions in equations (16) and (18) should be used instead. In other words, the fact that  $C_r^\infty = 0$  or  $C_r (\lambda \text{ large})$  is small does not imply that residual stresses can be ignored for thin adhesives.

### 3.4. Experimental suggestions

By using equation (22) with  $C_r$  determined by equation (16), it is possible to accurately determine  $G_I$  for any typical adhesive DCB specimen including the effect of residual stresses. There are two experimental problems when correcting for residual stresses. First, evaluation of  $C_r$  requires knowledge of  $\Delta\alpha$  and  $\Delta T$ . Second, even if  $\Delta\alpha$  and  $\Delta T$  are known, the form of  $C_r$  in equation (16) assumes that both the adhesive and adherend are linear thermoelastic materials with temperature-independent thermomechanical properties between  $T_0$  and  $T_s$  and that residual stresses are caused solely by differential thermal shrinkage. In real specimens, the thermomechanical properties will probably depend on temperature (especially in the adhesive near  $T_0$ ) and there may be additional sources of residual stresses such as chemical shrinkage during adhesive cure. This section suggests some experimental methods for accounting for residual stresses that will be valid for any form of residual stresses.

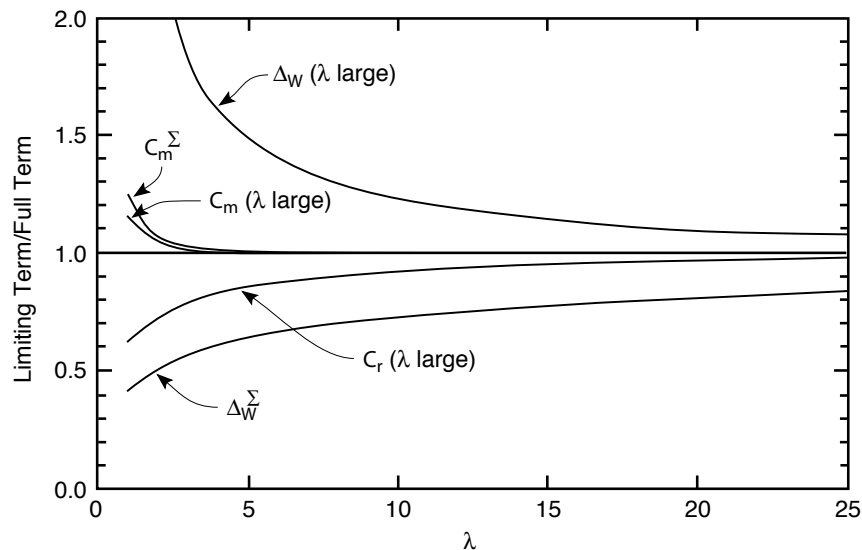


Fig. 5. Plots of  $C_m$  ( $\lambda$  large),  $C_m^\infty$ ,  $C_r$  ( $\lambda$  large),  $\Delta_W$  ( $\lambda$  large), and  $\Delta_W^\infty$  as a function of  $\lambda$ . Each constant has been normalized the the full beam analysis results ( $C_m$ ,  $C_r$ , and  $\Delta_W$ ). These plots are for an aluminum-epoxy specimen with  $R = 28$  and  $h = 5$  mm.

By equation (5), each arm of the adhesive DCB specimen is assumed to have an effective moment-curvature relation. In the absence of mechanical loads, the curvature due to residual stresses is

$$\kappa_{res} = \alpha_\kappa^* \Delta T \quad (30)$$

To account for any type of residual stresses, we simply repeat the previous analysis but use  $\kappa_{res}$  to calculate residual stress effects instead of  $\alpha_\kappa^* \Delta T$ . The result is that equations (7) and (8) change to

$$G_I = (C_m P a + C_{res})^2 \quad (31)$$

where

$$C_{res} = \frac{\kappa_{res}}{\sqrt{C_\kappa^* B}} = \frac{\kappa_{res} h_1}{2\lambda} \sqrt{\frac{E_1 h_1}{3} \frac{3(1+\lambda)^2 + (1+R\lambda) \left(\lambda^2 + \frac{1}{R\lambda}\right)}{1+R\lambda}} \quad (32)$$

The problem of accounting for residual stresses is reduced to experimentally finding  $\kappa_{res}$ ; some possible experimental methods are illustrated in *Figure 6*. The method in *Figure 6A* is to construct a calibration specimen for each adhesive DCB specimen and subject it to identical adhesive cure conditions. The calibration specimen is a two-layer, adhesive and adherend strip. Such an unbalanced structure will curve due to residual stresses. By measuring the chord length,  $l$ , and strip height,  $d$ , the residual stress curvature can be calculated from [17]

$$\kappa_{res} = \frac{2d}{d^2 + \frac{l^2}{4}} \quad (33)$$

The sign of  $\kappa_{res}$  is determined by the direction of curvature —  $\kappa_{res}$  is negative if the strip curves toward the adhesive and positive if it curves toward the adherend. Two drawbacks of using calibration specimens are that it requires preparing an extra specimen for each adhesive DCB specimen and that it may not be possible to subject the calibration specimens to identical cure conditions. Even when subjected to the same thermal history, the lack of an adherend on both sides of the adhesive may cause the calibration specimen to develop different residual stresses than the adhesive DCB specimen.

Prior to a test, the arms of an adhesive DCB specimen with residual stresses will have some initial curvature caused by those stresses. *Figures 6B* and *6C* show the possible types of initial arm curvature. This initial curvature could be used to determine  $\kappa_{res}$ . This approach avoids the need for construction of a

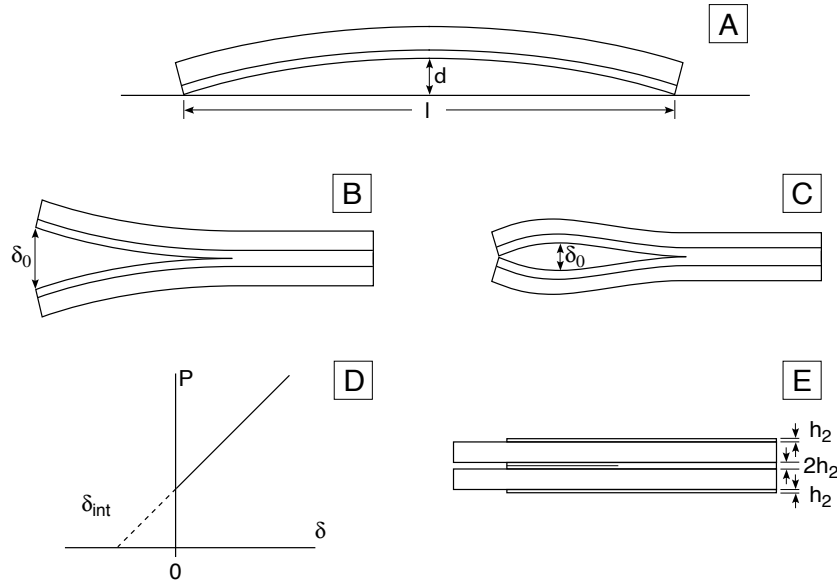


Fig. 6. Some experimental methods for determining the effect of residual stresses on  $G_I$  in adhesive DCB specimens. A. Measure the curvature of an unbalanced, two-layer, adhesive and adherend strip. B. Measure initial arm curvature when  $\kappa_{res} > 0$ . C. Measure initial arm curvature when  $\kappa_{res} < 0$ . D. Determine intercept in load-displacement curve. E. Prepare symmetric specimens.

second calibration specimen and guarantees that  $\kappa_{res}$  is measured from the correct cure conditions. *Figure 6B* corresponds to a specimen with  $\kappa_{res} > 0$ . For such specimens the arms will separate. From equation (6), the initial, total beam opening,  $\delta_0$ , is related to  $\kappa_{res}$  by

$$\delta_0 = a^2 \kappa_{res} \quad \text{or} \quad \kappa_{res} = \frac{\delta_0}{a^2} \tag{34}$$

*Figure 6C* corresponds to a specimen with  $\kappa_{res} < 0$ . For such specimens, the arms will bend towards each other, but the arm ends will contact each other, inducing a load that prevents interpenetration. Integration of equation (5) and evaluation of the load  $P$  ( $M = Px$ ) required for zero displacement at  $x = 0$  shows that the maximum arm separation occurs at  $x = a/3$ . The maximum separation,  $\delta_0$ , is related to  $\kappa_{res}$  by

$$\delta_0 = -\frac{2a^2 \kappa_{res}}{27} \quad \text{or} \quad \kappa_{res} = -\frac{27\delta_0}{2a^2} \tag{35}$$

Notice that for specimens with identical magnitudes of  $\kappa_{res}$ , the maximum arm separation used for determination of  $\kappa_{res}$  is more than an order of magnitude smaller when  $\kappa_{res} < 0$  than it is when  $\kappa_{res} > 0$ . This observation has two consequences. First, it may be difficult to accurately measure  $\kappa_{res}$  when it is negative; this drawback is particularly troublesome because  $\kappa_{res}$  is negative for most adhesive specimens. Second, an observation that there is not much initial curvature in the arms of an adhesive DCB specimen with  $\kappa_{res} < 0$  is not sufficient justification for ignoring residual stresses in that specimen.

Perhaps a better way to measure  $\kappa_{res}$  from the adhesive DCB specimen itself is to extract it from a measured load-displacement curve. *Figure 6D* shows an expected load-displacement curve where the displacement is the total arm displacement between the bottom surfaces of the arms measured at the loading points ( $x = 0$ ). This curve is for an adhesive specimen with negative  $\kappa_{res}$ ; the non-zero load at zero displacement is the load induced that prevents arm penetration. By extrapolation of the linear load-displacement curve with positive displacements to zero load, it is easy to show that the intercept,  $\delta_{int}$ , is related to  $\kappa_{res}$  by

$$\delta_{int} = a^2 \kappa_{res} \quad \text{or} \quad \kappa_{res} = \frac{\delta_{int}}{a^2} \tag{36}$$

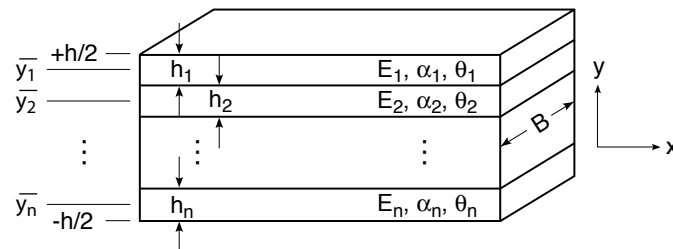


Fig. 7. The coordinate system used for laminated beam analysis of one arm of an laminate DCB delamination specimen.

The extrapolation method works equally when for  $\kappa_{res} > 0$  and  $\kappa_{res} < 0$ . The only difference is that when  $\kappa_{res} < 0$ , the extrapolation must be done from positive displacements, which can be measured, into negative displacements, which cannot be measured. The only drawback of this intercept-extrapolation method is that it requires the extra effort of accurately measuring beam opening during the experiments. The measured displacement must also be accurately calibrated to give zero displacement when the beam arms touch.

Many adhesive specimens have an adhesive drop-off before the end of the specimen, as illustrated by the zone of length  $b$  in *Figure 1*. The extrapolation method can be modified to handle such specimens. Integration of the beam moment-curvature relation with allowance for a change in beam properties at  $x = b$  gives the intercept of the load displacement curve as

$$\delta_{int} = 2h_2 + (a^2 - b^2)\kappa_{res} \quad \text{or} \quad \kappa_{res} = \frac{\delta_{int} - 2h_2}{a^2 - b^2} \quad (37)$$

Here  $2h_2$  is the additional beam opening at the loading point because there is no adhesive present and the  $(a^2 - b^2)$  term corrects for the reduced length of the zone with adhesive. When  $\kappa_{res} < 0$ , the extrapolation must be made from displacements greater than  $2h_2$ .

The final experimental suggestion for dealing with residual stresses is to prepare specimens with no residual stress effect. As explained above, the entire effect of residual stresses can be traced to external work done by the arms as they curve due to the presence of residual stresses. This curvature can be eliminated by constructing symmetric DCB arms. As shown in *Figure 6E*, symmetric arms can be made by adding a layer of adhesive of thickness  $h_2$  to both the top and bottom surfaces of the adhesive DCB specimen. The residual stresses can be ignored in the analysis of such a specimen. Three drawbacks of symmetric arms are that they complicate specimen fabrication, that the thickness of the outer layers must be carefully controlled to  $h_2$  (or half to total adhesive joint thickness), and that the cure conditions must guarantee that the adhesive on the surfaces develop an identical level of residual stresses as the adhesive joint.

#### 4. Laminate double cantilever beam specimens

Another application of double cantilever beam specimens is to measure mode I delamination toughness of composite laminates [5]. By starting from equations (7) and (8), solving the laminate problem for energy release rate including the effect of residual stresses is simply a matter of determining  $C_\kappa^*$  and  $\alpha_\kappa^*$  for each arm of the laminate specimen. A simple laminated beam analysis of the single DCB arm in *Figure 7* is given in the *Appendix*; substituting those results for  $C_\kappa^*$  and  $\alpha_\kappa^*$  into equation (8) gives the required  $C_m$  and  $C_r$  needed to for total  $G_I$ . This plane-stress, laminate analysis treats the composite arms as beams. It therefore ignores possible anti-clastic curvature and bending-twisting coupling effects [18, 19].

As with adhesive DCB specimens, the simple beam theory result for  $C_m$  is not very accurate and needs to be corrected for beam rotation effects. As with the adhesive DCB specimen, that correction can be done by introducing an effective crack length as has been discussed by Williams [11]. Because laminate DCB arms are orthotropic materials, the  $C_m$  correction differs from the one for adhesive DCB specimen with isotropic arms [11]. The remainder of this section will only consider the effects of residual stresses and suggest experimental methods for accounting for residual stresses. Each of these topics can be analyzed accurately without knowledge of the correction factors required for  $C_m$ .

Table 1. Errors caused by ignoring residual stresses in delamination experiments on a series of graphite/epoxy laminates. The experiments are assumed to be on 16-ply laminates with delamination in the middle of the laminate. The laminates listed here are the layups for the 8-ply laminates in each DCB specimens.

8-Ply Arm Layup	$G_{IC}$ Error (%)	8-Ply Arm Layup	$G_{IC}$ Error (%)
[0 <sub>8</sub> ]	0.00	[0 <sub>2</sub> /90 <sub>2</sub> /0 <sub>2</sub> /90 <sub>2</sub> ]	+15.33
[90/0 <sub>7</sub> ]	-6.21	[0/90/0/90/0/90/0/90]	+7.09
[90 <sub>2</sub> /0 <sub>6</sub> ]	-14.59	[90/0/90/0/90/0/90/0]	-6.84
[90 <sub>4</sub> /0 <sub>4</sub> ]	-37.68	[90 <sub>2</sub> /0 <sub>2</sub> /90 <sub>2</sub> /0 <sub>2</sub> ]	-14.24
[90 <sub>6</sub> /0 <sub>2</sub> ]	-54.85	[0 <sub>2</sub> /90 <sub>2</sub> /45 <sub>2</sub> / - 45 <sub>2</sub> ]	+47.00
[90 <sub>8</sub> ]	0.00	[90 <sub>2</sub> /0 <sub>2</sub> /45 <sub>2</sub> / - 45 <sub>2</sub> ]	+15.64
[0 <sub>2</sub> /90 <sub>6</sub> ]	+76.36	[0 <sub>2</sub> /45 <sub>2</sub> / - 45 <sub>2</sub> /90 <sub>2</sub> ]	+61.11
[0 <sub>4</sub> /90 <sub>4</sub> ]	+46.34	[90 <sub>2</sub> /45 <sub>2</sub> / - 45 <sub>2</sub> /0 <sub>2</sub> ]	-46.60
[0 <sub>6</sub> /90 <sub>2</sub> ]	+15.75	[45 <sub>2</sub> / - 45 <sub>2</sub> /0 <sub>2</sub> /90 <sub>2</sub> ]	-14.51
[0 <sub>7</sub> /90]	+6.41	[-45 <sub>2</sub> /45 <sub>2</sub> /90 <sub>2</sub> /0 <sub>2</sub> ]	-37.97

#### 4.1. Consequence of ignoring residual stresses

From equation (24), the error caused by ignoring residual stresses is a function only of  $C_r$ ,  $\Delta T$ , and  $G_{IC}$ . We considered a series of graphite/epoxy laminates with  $G_{IC} = 200 \text{ J/m}^2$  and  $\Delta T = -125^\circ\text{C}$ , which are typical values for graphite epoxy laminates [20–22]. The value of  $C_r$  depends on the layup of the specimen arms and can be calculated by the laminated beam analysis in the *Appendix* followed by substitution into equation (8). *Table 1* lists the error caused by ignoring residual stresses for delamination down the middle of a series of 16-ply laminates which leads to 8-ply laminate DCB arms. In all examples, the undelaminated 16-ply laminate is symmetric; the 8-ply arms, however, may be unsymmetric. The ply properties used in these calculations were  $E_1 = 138000 \text{ MPa}$ ,  $E_2 = 8970 \text{ MPa}$ ,  $\nu_{12} = 0.30$ ,  $G_{12} = 6900 \text{ MPa}$ ,  $\alpha_1 = -0.04 \times 10^{-6} \text{ K}^{-1}$ ,  $\alpha_2 = 18.0 \times 10^{-6} \text{ K}^{-1}$ , and  $h_i = 0.127 \text{ mm}$ .

The first column of *Table 1* gives a series of DCB arms with  $0^\circ$  and  $90^\circ$  plies. The two special cases of [0<sub>8</sub>] and [90<sub>8</sub>] are not affected by residual stresses and thus introduce no error. The arms in these specimens are themselves symmetric laminates and therefore do not curve due to residual stresses. Because there is no thermal curvature, there is no external work due to residual stresses and no residual stress effect on  $G_I$ . These layups will have residual stresses caused by differential shrinkage between the fibers and the matrix. These residual stresses, however, do not release any energy as the delamination crack propagates. Many previous delamination experiments have been done on unidirectional laminates. It is correct to ignore residual stresses when analyzing such experiments.

All other arrangements of  $0^\circ$  and  $90^\circ$  plies, besides [0<sub>8</sub>] and [90<sub>8</sub>], have an effect of residual stresses that cannot be ignored. The smallest error, caused by a change of a single ply on the surface, is 6.21% ([90/0<sub>7</sub>]); the largest error is 76.36% ([0<sub>2</sub>/90<sub>6</sub>]). An interesting example is the [0<sub>4</sub>/90<sub>4</sub>] laminate. If the delamination growth is parallel to the fibers in the surface plies, the apparent  $G_{IC}$  will be 46.54% too high (293  $\text{J/m}^2$  in this example). But, if the laminate is rotated  $90^\circ$  and the delamination is propagated parallel to the fibers in the central plies, the apparent  $G_{IC}$  will be 37.68% too low (125  $\text{J/m}^2$  in this example). The two apparent toughnesses will differ by more than a factor of two.

The second column of *Table 1* lists some alternate layups with four  $0^\circ$  and four  $90^\circ$  plies and lists some quasi-isotropic layups. Among the 0/90 laminates, the sign of the error depends on the stacking sequence and the magnitude depends on the ply groupings. Positive errors result when the  $90^\circ$  plies are in the middle while negative errors result when  $0^\circ$  plies are in the middle. The errors get smaller as the ply groupings get smaller; the smallest error is for alternating  $0^\circ$  and  $90^\circ$  plies. Among the quasi-isotropic layups, the error ranges from -46.60% to +61.11%. It is not possible to construct laminate arms made from 0<sub>2</sub>, 90<sub>2</sub>, 45<sub>2</sub>, and -45<sub>2</sub> ply pairs having a residual stress effect that causes less than a 14% error. If the ply pairs are split apart, the errors can be made smaller. Symmetric arm layups such as [0/90/ + 45/ - 45/ - 45/ + 45/90/0]

would have no residual stress effects.

#### 4.2. Experimental suggestions

Rather than calculate  $C_r$  from laminated plate or beam theory and knowledge of  $\Delta T$ , it is preferable to experimentally correct for residual stresses. As with adhesive DCB specimens, experimental correction avoids having to measure additional thermomechanical properties and furthermore can account for residual stresses caused by any mechanisms. As with adhesive DCB specimens, residual stress curvature in laminate DCB specimens can be evaluated by using calibration specimens (*Figure 6A*), by measuring initial arm curvature (*Figures 6B* and *6C*), or by extrapolating from carefully-zeroed, load-displacement results (*Figure 6D*). The extrapolation method is probably the best method.

Also like adhesive DCB specimens, the residual stress effect can be eliminated by use of specimens with symmetric arms [18, 19] (*Figure 6E*). This approach is more attractive in delamination specimens than in adhesive specimens because instead of the extra work of adding layers and carefully controlling their thickness, it only requires selecting specimens with a doubly-symmetric layup. Here, a double-symmetric layup is a symmetric laminate for which each delaminating arm is itself a symmetric laminate. The absence of a residual stress effect in doubly-symmetric laminates assumes the laminate was cooled slow enough such that there are no residual stresses due to thermal gradients during cooling. A specimen that is cooled rapidly would probably develop compressive stresses on the surface and tensile stresses in the middle. Such a distribution of residual stresses would cause the arms to curve away from each other as they delaminate or act like a specimen with  $\kappa_{res} > 0$  and give an apparent toughness that is lower than the true toughness. Because thermal gradient effects become larger as the laminate gets thicker, compression on the outside and tension in the middle would cause the toughness to *decrease* as the specimens get thicker. Because the axial thermal expansion coefficient of many unidirectional carbon-fiber laminates is negative, an opposite situation would occur for delamination parallel to the fibers. Rapid cooling would cause tension on the outside and compression in the middle and the apparent toughness would *increase* as the specimens got thicker. Indeed, the apparent toughness of unidirectional IM6 carbon fiber/PEEK specimens has been observed to increase with arm thickness [23]. This observation, however, was attributed to fiber bridging instead of residual stresses [23]. That conclusion is supported by the extra experiments in Ref. 23 that showed that the toughness did not change as the cooling rate increased.

#### Acknowledgements

This work was supported by a grant from the Mechanics of Materials program at the National Science Foundation CMS-9713356.

#### Appendix A

The effective properties of a laminate DCB specimen can be determined from laminated plate theory. Here, however, all analyses are plane-stress, beam analyses and therefore a laminated beam theory was used. For the laminate arm illustrated in *Figure 7* under axial strain  $\varepsilon_0$  and curvature  $\kappa$ , the axial strain as a function of  $y$  is

$$\varepsilon(y) = \varepsilon_0 - \kappa y \quad (38)$$

where  $\kappa > 0$  corresponds to curvature upward. The axial stress in each layer, including residual stresses, is

$$\sigma(y) = E(y)(\varepsilon_0 - \kappa y - \alpha(y)\Delta T) \quad (39)$$

where  $E(y)$  and  $\alpha(y)$  are the position-dependent modulus and thermal expansion coefficient in the  $x$  direction. Integrating these stresses, the total axial force,  $F$ , and bending moment,  $M$ , can be written as

$$F = A_{11}\varepsilon_0 - B_{11}\kappa - N_T\Delta T \quad \text{and} \quad M = -B_{11}\varepsilon_0 + D_{11}\kappa + M_T\Delta T \quad (40)$$

where

$$A_{11} = B \int_{-h/2}^{h/2} E(y) dy = B \sum_{i=1}^n E(\theta_i) h_i \quad (41)$$

$$B_{11} = B \int_{-h/2}^{h/2} y E(y) dy = B \sum_{i=1}^n E(\theta_i) h_i \bar{y}_i \quad (42)$$

$$D_{11} = B \int_{-h/2}^{h/2} y^2 E(y) dy = B \sum_{i=1}^n E(\theta_i) h_i \left( \bar{y}_i^2 + \frac{h_i^2}{12} \right) \quad (43)$$

$$N_T = B \int_{-h/2}^{h/2} E(y) \alpha(y) dy = B \sum_{i=1}^n E(\theta_i) \alpha(\theta_i) h_i \quad (44)$$

$$M_T = B \int_{-h/2}^{h/2} y E(y) \alpha(y) dy = B \sum_{i=1}^n E(\theta_i) \alpha(\theta_i) h_i \bar{y}_i \quad (45)$$

$$(46)$$

Here  $E(\theta_i)$ ,  $\alpha(\theta_i)$ ,  $h_i$ , and  $\bar{y}_i$  are the  $x$ -direction modulus,  $x$ -direction thermal expansion coefficient, thickness, and midpoint of ply  $i$  with orientation angle  $\theta_i$ .  $A_{11}$ ,  $B_{11}$ , and  $D_{11}$  are the (1,1) elements of the usual laminated plate theory  $A$ ,  $B$ , and  $D$  matrices except for the extra factor of  $B$  because  $F$  and  $M$  are total forces and moments instead of force and moment resultants. By the usual rules for rotation of thermomechanical properties,  $E(\theta_i)$  and  $\alpha(\theta_i)$  are

$$\frac{1}{E(\theta_i)} = \frac{\cos^4 \theta_i}{E_1} + \left( \frac{1}{G_{12}} - \frac{2\nu_{12}}{E_1} \right) \sin^2 \theta_i \cos^2 \theta_i + \frac{\sin^4 \theta_i}{E_2} \quad (47)$$

$$\alpha(\theta_i) = \alpha_1 \cos^2 \theta_i + \alpha_2 \sin^2 \theta_i \quad (48)$$

Here  $E_1$ ,  $E_2$ ,  $G_{12}$ ,  $\nu_{12}$ ,  $\alpha_1$ , and  $\alpha_2$  are the in-plane tensile and shear moduli, Poisson's ratio, and thermal expansion coefficients of the ply material with 1 being the fiber direction and 2 being the transverse direction. Finally, setting  $F = 0$  and solving for  $\kappa$  gives

$$\kappa = C_\kappa^* M + \alpha_\kappa^* \Delta T \quad (49)$$

where the effective beam properties are

$$C_\kappa^* = \frac{A_{11}}{A_{11} D_{11} - B_{11}^2} \quad \text{and} \quad \alpha_\kappa^* = \frac{B_{11} N_T - A_{11} M_T}{A_{11} D_{11} - B_{11}^2} \quad (50)$$

## References

- [1] Ripling, E. J., S. Mostovoy, and R. L. Patrick *Materials Research & Standards* 1964, **4**, 129–134.
- [2] Mostovoy, S. and E. J. Ripling *J. Appl. Polym. Sci.* 1966, **10**, 1351–1374.
- [3] Mostovoy, S. and E. J. Ripling *J. Appl. Polymer Sci.* 1971, **15**, 661–673.
- [4] ASTM D3433-93, in *Annual Book of ASTM Standards* 1996, **15.06**, 215–221.
- [5] ASTM D5528-94a, in *Annual Book of ASTM Standards* 1996, **15.03**, 280–288.
- [6] Reeder, J. R. and J. H. Crews, Jr. *AIAA J.* 1990, **28**, 1270–1276.
- [7] Hashemi, S., A. J. Kinloch, and J. G. Williams *Proc. R. Soc. Lond.* 1990, **A347**, 173–199.
- [8] Blackman, B., A. J. Kinloch, and J. G. Williams, personal communication.
- [9] Williams, J. G. *J. Comp. Mater.* 1987, **21**, 330–347.
- [10] Williams, J. G. in *Proc. Int'l Mechanical Engineering Congress and Exhibition: The Winter Annual Meeting of the ASME, Symposium on Mechanics of Plastics and Plastic Composites* 12–17 November 1995, San Francisco, USA.
- [11] Williams, J. G. *Comp. Sci. & Tech.* 1989, **35**, 367–376.

- [12] Nairn, J. A. *J. Applied Mech.* 1997, **64**, 804–810.
- [13] Crandall, S. H., N. C. Dahl, and T. J. Lardner, *An Introduction to the Mechanics of Solids*, McGraw-Hill Book Company, New York (1978).
- [14] Timoshenko, S. *J. Opt. Soc. Amer.* 1925, **11**, 233–256.
- [15] Krishnamurthy, T., Ramamurthy, T. S., Vijayakumar, K. and Dattaguru, B. in ‘Proc. Int. Conf. Finite Elements in Computational Mechanics’, 2-6 December 1985, Bombay, India, 891–900.
- [16] Kanninen, M. F. *Int. J. Fract.* 1973, **9**, 83–92.
- [17] Nairn, J. A. and P. Zoller *ASTM STP 937* 1987, 328–341.
- [18] Hudson, R. C., B. D. Davidson, and J. J. Polaha *Proc. ICCM-10* 1995, **I**, 133–140.
- [19] Polaha, J. J., B. D. Davidson, R. C. Hudson, and A. Pieracci *J. Reinforced Plast. and Comp.* 1996, **15**, 141–173.
- [20] Hunston, D. L. *Comp. Tech. Rev.* 1984, **6**, 176–180.
- [21] Hunston, D. L., R. J. Moulton, N. J. Johnston, and W. D. Bascom in *Toughened Composites*, ed. N. J. Johnston 1987, **ASTM STP 937**, 74–94.
- [22] Liu, S. and J. A. Nairn *J. Reinf. Plast. & Comp.* 1992, **11**, 158–178.
- [23] Davies, P., W. Cantwell, C. Moulin, and H. H. Kausch *Comp. Sci. & Tech.* 1989, **36**, 153–166.